AGU PUBLICATIONS

Geophysical Research Letters

RESEARCH LETTER
10.1002/2016GL069573

Key Points:
- There is a 120 day Rossby wave resonant mode in the Caribbean Sea
- The mode strongly affects coastal sea level and dominates bottom pressure
- The mode operates in a manner dynamically equivalent to a whistle

Supporting Information:
- Supporting Information S1
- Movie S1

Correspondence to:
C. W. Hughes,
cwh@liv.ac.uk

Citation:
Hughes, C. W., J. Williams, A. Hibbert, C. Boening, and J. Oram (2016), A Rossby whistle: A resonant basin mode observed in the Caribbean Sea, *Geophys. Res. Lett.*, *43*, 7036–7043, doi:10.1002/2016GL069573.

Received 12 MAY 2016
Accepted 13 JUN 2016
Accepted article online 19 JUN 2016
Published online 2 JUL 2016

A Rossby whistle: A resonant basin mode observed in the Caribbean Sea

Chris W. Hughes[1,2], Joanne Williams[2], Angela Hibbert[2], Carmen Boening[3], and James Oram[1]

[1]School of Environmental Sciences, University of Liverpool, Liverpool, UK, [2]National Oceanography Centre, Liverpool, UK, [3]2 Jet Propulsion Laboratory, California Institute of Technology, Pasadena, California, USA

Abstract We show that an important source of coastal sea level variability around the Caribbean Sea is a resonant basin mode. The mode consists of a baroclinic Rossby wave which propagates westward across the basin and is rapidly returned to the east along the southern boundary as coastal shelf waves. Almost two wavelengths of the Rossby wave fit across the basin, and it has a period of 120 days. The porous boundary of the Caribbean Sea results in this mode exciting a mass exchange with the wider ocean, leading to a dominant mode of bottom pressure variability which is almost uniform over the Grenada, Venezuela, and Colombia basins and has a sharp spectral peak at 120 day period. As the Rossby waves have been shown to be excited by instability of the Caribbean Current, this resonant mode is dynamically equivalent to the operation of a whistle.

1. Introduction

The Caribbean Sea is a semienclosed basin with multiple, connected deep basins. Figure 1a shows the geography of the region and the position of a bottom pressure recorder (BPR), as well as two high-quality tide gauges. *Williams et al.* [2014] found that this BPR showed more energetic bottom pressure variability than other tropical regions and that model predictions failed to remove that variability. Investigation of the cause of that bottom pressure signal led us to the conclusions presented in this paper.

Large bottom pressure fluctuations are found in other semienclosed basins, most notably in the Arctic [*Hughes and Stepanov*, 2004; *Peralta-Ferriz et al.*, 2011; *Volkov and Landerer*, 2013], where the variability is highly coherent across the whole basin. *Fukumori et al.* [2015] showed clearly that the Arctic mode is excited by the interaction of winds and continental shelf waves. These act to pump water into or out of the basin along the shelf and upper continental slope, with a rapid homogenization of the resulting pressure signal over the deep basin. Thus, we can expect (and model studies shown below confirm this) that the bottom pressure signal in the Caribbean Sea will be dominated by a uniform signal over the deep basin, controlled by mass exchange with the surrounding ocean. The main question is what controls that mass exchange.

As we will show, a large fraction of the bottom pressure variability in the Caribbean Sea is in a sharply resonant mode with a period of 120 days. The excitation of this mode is ultimately derived from instability of the Caribbean Current which flows through the basin, as seen (Figure 1b) in sea level observations from the Aviso gridded satellite altimetry product [http://www.aviso.altimetry.fr/]. We will first explore how the mode appears in ocean models, then show the observational evidence for the mode, and finally interpret the dynamics of the mode.

2. The Caribbean Sea Basin Mode in Ocean Models

We analyzed the Caribbean sea level and ocean bottom pressure in four different ocean models, the results from all of which were very similar. The data used are from years 1988–2006 inclusive of the 1/12° resolution OCCAM model [*Marsh et al.*, 2009], years 1979–2010 from the 1/12° NEMO model NEMO12 and years 1958–2007 from the 1/4° NEMO model NEMOq [*Blaker et al.*, 2014], and years 1992–2013 from the eddy-permitting Jet Propulsion Laboratory (JPL) ECCO2 model [*Menemenlis et al.*, 2005a, 2005b]. The latter is a data-assimilating model in which model parameters have been tuned by comparison with satellite altimetry and other measurements. Apart from this tuning, all four model runs are freely running ocean models with prescribed atmospheric forcing based on atmospheric reanalyses, excluding atmospheric pressure. In order to

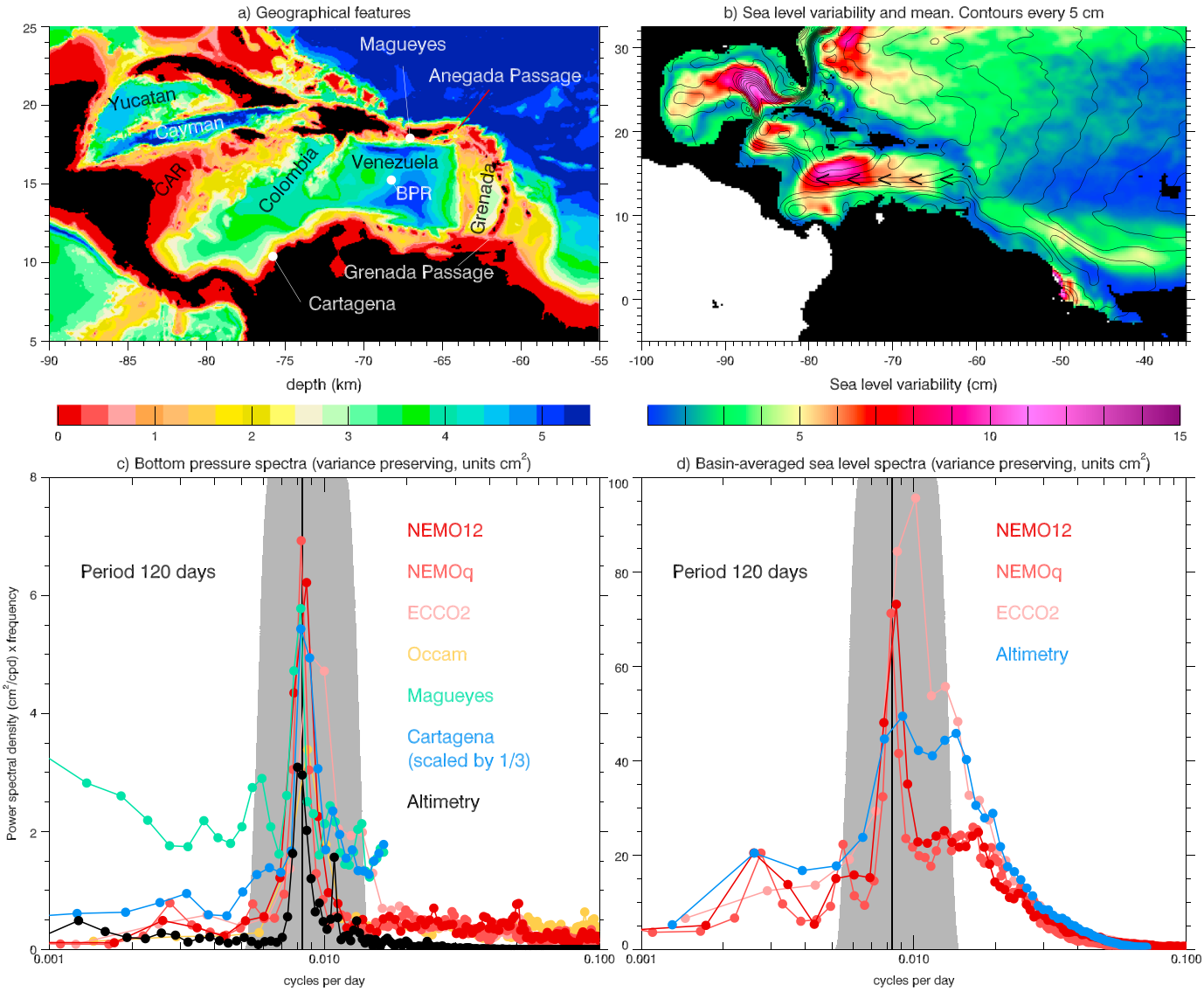

Figure 1. (a) Geographical features including ocean depth [*IHO, IOC and BODC*, 2003] and names of basins referred to in this paper. CAR is Central American Rise, and BPR is the position of the Bottom Pressure Recorder. (b) Standard deviation of sea level in the 75–175 day period band (colors) and contours of mean dynamic topography, from Aviso altimetry products. Arrows mark the Caribbean Current. (c) Spectra of bottom pressure from the BPR site in four ocean models (red to orange), from inverse barometer-corrected tide gauge data at Magueyes and Cartagena and predicted from satellite altimetry (see section 3). Spectra are plotted in variance-preserving form, and the power is divided by three in the case of Cartagena. The 75–175 day band-pass filter is shown in grey, multiplied by 8. (d) Basin-averaged variance-preserving spectra of sea level variability from three ocean models (red) and from Aviso satellite altimetry. Spectra are averaged over regions deeper than 1400 m in the Grenada, Venezuela and Colombia basins. The renormalized band-pass filter is again shown in grey.

ensure global ocean mass conservation, we calculate the global ocean average of bottom pressure and subtract it off at each time. A consistent correction is also applied to sea level. Bottom pressure spectra from the position of the BPR are shown in variance-preserving form in Figure 1c. All four models show a well-defined peak in energy at a period of around 120 days, with ECCO2 showing a broader peak than the other models, and more energy at shorter periods out to about 60 days. This sharp peak immediately shows that wind stress is not the main driver, as there is no corresponding peak in atmospheric variables.

Sea level spectra averaged over the Grenada, Venezuela, and Colombia basins are shown in Figure 1d. Sea level is substantially more energetic than bottom pressure, especially at periods of about 100 to 50 days (frequencies 0.01–0.02 cycles per day), but all show some evidence of the resonant peak, including satellite altimetry, though the peak in altimetry is much less prominent compared to the broad, presumably mesoscale

variability at shorter periods. The tuning of ECCO2 against altimeter observations may partly explain why it has different sea level and bottom pressure spectra compared to the other models.

Focusing on this spectral peak, we applied a band-pass filter to the bottom pressure and sea level. Shown in grey on Figure 1, the filter is a smoothed boxcar, with a (1 + cosine) taper of width 10% of the cutoff frequencies and has half amplitude at periods 75 and 175 days. The band-passed bottom pressure time series are not very strongly correlated between models, giving correlations between 0.13 and 0.42 for overlap periods of between 15 and 29 years. This implies that the spectral peak is produced by predominantly stochastic variability, although the fact that all correlations are positive does suggest a degree of phase locking so that wind stress and/or the seasonal cycle may play a weak role.

All the models show very similar dynamics, so we will present in more detail representative results from just the NEMO12 model. We find that bottom pressure is highly correlated over the Grenada, Venezuela, and Colombia basins, so we use as a reference time series the pressure averaged over these basins where they are more than 1400 m deep. The overall result is most clearly illustrated by correlating and least squares fitting sea level and bottom pressure at each point, on this basin average bottom pressure (all band-pass filtered as above), as shown in Figure 2. In order to account for lags in the predominantly cyclic time series, we use complex time series in which the imaginary component is simply a copy of the real component with each Fourier component shifted by 90° in phase (a Hilbert transform). The real part of the correlation or fit, amplitude × cosine of the phase, represents a fit on the basin average with no lag; the imaginary part, amplitude × sine of the phase, represents a fit at 90° phase lag.

For bottom pressure, there is very strong correlation with near-constant amplitude and very small lag over the Grenada, Venezuela, and Colombia basins. Weaker signals extend into the Cayman and Yucatan basins, and more weakly into the Gulf of Mexico. The most obviously different region is along the southern and western boundary of the southern basins. Here there is a phase lag of 180° over the Central American Rise, with the lag becoming less negative farther east and into shallower water. More detailed analysis (see Supporting Information S1) shows that the minimum amplitude and 90° phase lie approximately along the 400 m isobath on most of this coastline. This resembles the Arctic situation in that bottom pressure is dominated by a mode which is uniform over the deep basin, and the continental shelf and slope seems to play an important role.

To give an idea of the size of the variability, the standard deviation of basin-averaged bottom pressure in NEMO12 is 1.56 cm (sea level equivalent), reducing to 1.14 cm after filtering, with values 10–15% higher in ECCO2. With a period of 120 days, a 1 cm amplitude signal requires an oscillating inflow/outflow of amplitude about 0.0084 Sv (1 Sv = 1 sverdrup = 10^6 m^3 s^{-3}), over a thousand times smaller than the observed and modeled variations in flows through individual passages [*Johns et al.*, 2002], which shows how precisely balanced the inflows and outflows are at any one time. Nonetheless, this is a very clear bottom pressure signal and much larger than those seen at similar latitudes elsewhere in the deep ocean.

Sea level is necessarily very similar to bottom pressure at the coast but shows very different behavior in deep water, where the amplitudes are much larger than those for bottom pressure. There are still strong correlations, particularly along and south of the path of the Caribbean Current. However, the phase shows that this represents a westward propagating signal with almost two wavelengths along the length of the basin. A (necessarily approximate) estimate of the wavelength is 1100 km, and the basin width suggests a meridional half wavelength of about 600 km. With a first baroclinic Rossby radius R_1 of 80 km, and typical meridional gradient of the Coriolis parameter $\beta = 2.2 \times 10^{-11}$ m^{-1} s^{-1} [*Jouanno et al.*, 2009], we can substitute these values into the linear Rossby wave dispersion relation ($\omega = -\beta k/[k^2 + l^2 + 1/R_1^2]$, where k and l are zonal and meridional angular wave numbers, respectively, and ω is the angular frequency), to obtain a predicted wave period of 125 days (shorter if the zonal wavelength is shorter, but longer if the meridional wavelength is shorter) and a propagation speed of 10 cm s^{-1}. The sea level pattern therefore has the nature of a baroclinic Rossby wave.

The combined effect of amplitude and phase can be seen in an animation of the cyclic fits (see the supporting information). In sea level, we see a baroclinic Rossby wave which grows as it propagates to the west across the Venezuela and Colombia basins. A small part of this wave leaks through to the Cayman basin, but most of it appears to fade away as it reaches the Central American Rise. Looking at bottom pressure, we see that the baroclinic nature of the Rossby wave is reflected in the opposing phases of bottom pressure in shallow and deep parts of the Central American Rise. That opposing phase pattern propagates rapidly to the east along the continental slope, but only the deep part of the signal remains trapped in the basin, with the shallow

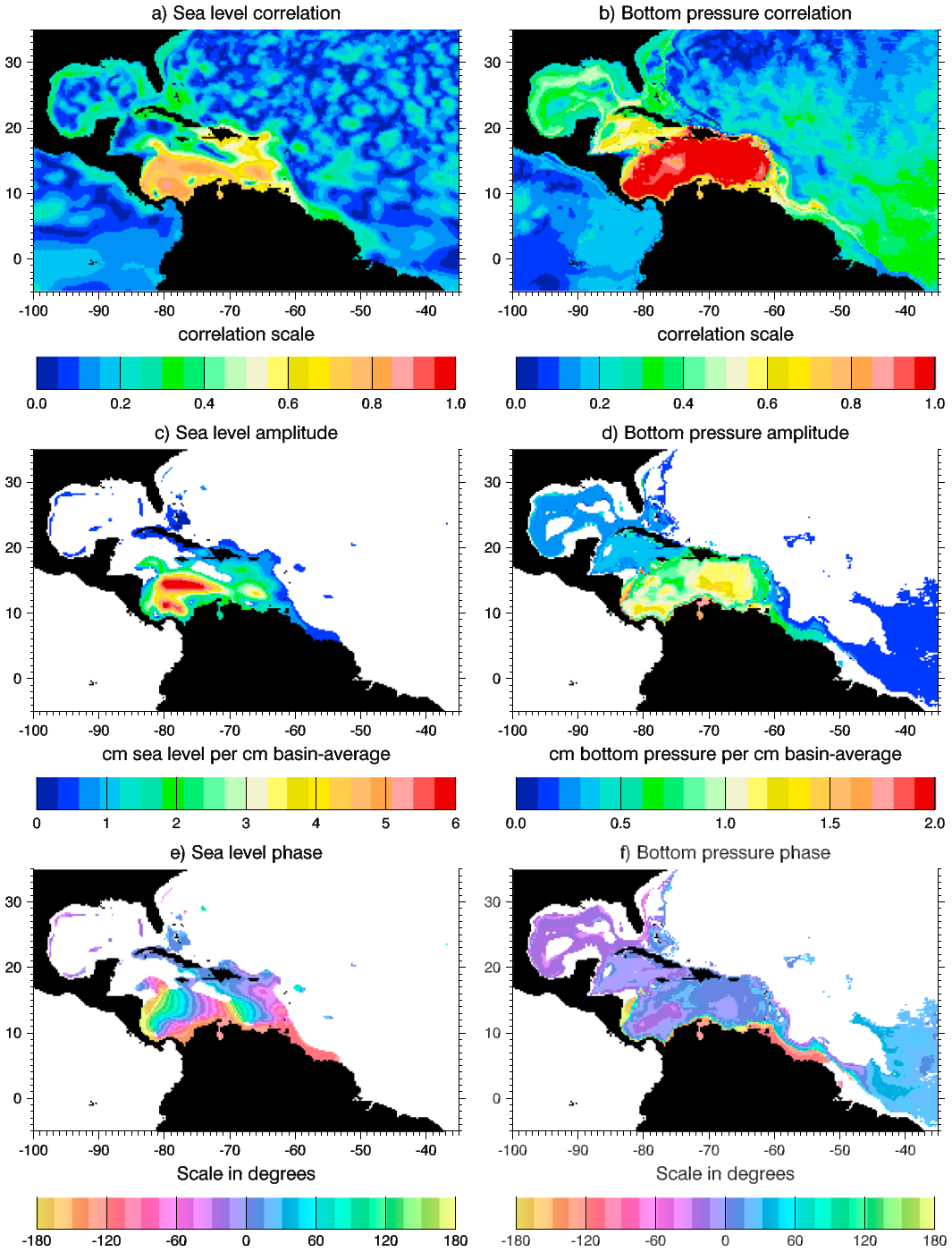

Figure 2. Amplitude of (a, b) the complex correlation, and (c, d) the complex fit of sea level (Figures 2a and 2c) and bottom pressure (Figures 2b and 2d) on basin-averaged bottom pressure in the NEMO12 model. (e,f) The corresponding phase. All time series are band-pass filtered in the 75–175 day band and made complex using a Hilbert transform. Phase is zero for a time series which peaks at the same time as the basin-averaged time series, and small positive phase means that the peak follows the basin average. For the fit and the phase, regions where the complex correlation coefficient amplitude is below 0.3 are left white.

part propagating out along the coast. Sea level also suggests the excitation of a secondary Rossby wave propagating across the southern end of the Colombia basin.

We can demonstrate that the sea level and bottom pressure signals are parts of a single mode, rather than separately representing variability at a 120 day period that happens by chance to be correlated. Using the fit of basin-averaged pressure on sea level (i.e., the opposite way round to the fit shown in Figure 2) allows an estimate of bottom pressure from sea level at each grid point. To make use of all the data, we average the estimates based on sea level from all points within 2.5° of the deep basin. This produces a time series which has a correlation of 0.94 with the filtered, basin-averaged bottom pressure. If we now use the same weightings derived from the NEMO12 model to infer bottom pressure in ECCO2 from sea level in ECCO2, we obtain a basin-averaged bottom pressure prediction for ECCO2 which also has a 0.94 correlation with the true, band-passed model pressure and is very close to the correct amplitude, explaining 86% of the variance without further scaling. The actual time series are shown in the supporting information. This is far better than can be expected by chance and demonstrates that the nature of the link between sea level and bottom pressure is very similar between the two models. The robustness of this calculation means that we also have a way of inferring basin-averaged bottom pressure variations in the real ocean from satellite altimetry.

3. Comparison With Observations

The method described above produces a prediction of basin-averaged bottom pressure from the Aviso altimetry, which only involves using spatial patterns taken from the NEMO12 model. The spectrum of this predicted time series, shown in Figure 1c, shows a very sharp peak at a 120 day period, confirming that the resonance is observed. In Figure 3a (black), we show the corresponding time series after filtering. As we will be comparing this with some rather gappy data sets, this has been filtered using a robust approximation of the band-pass filter which consists of removing a least squares fit of trend, annual and semiannual, followed by convolution with the difference of Gaussian kernels of width 60 and 200 days (twice the width at half amplitude). We compare this with two estimates of bottom pressure from the region.

The first is a repeated BPR deployment in the Venezuela basin (labeled "BPR" in Figure 1a) as part of the National Tsunami Hazard Warning System [*Gonzalez et al.*, 2005]. This was downloaded as daily mean values from the Permanent Service for Mean Sea Level (PSMSL). We remove tides and drift from the BPR data as described by *Williams et al.* [2014], and apply the robust filter. The result is shown in blue in Figure 3a. The resulting time series has a correlation of 0.66 with the altimeter prediction and explains 43% of the predicted variance without scaling, rising to a maximum of 44% if we multiply the prediction by 0.92. We assess significance by comparing with correlations at different lags. We find the absolute correlation has 146 peaks over the range of lags available, of which the largest magnitude correlations are 0.67 at lag −1 days and −0.64 at 53 days, so this correlation is significant at least at the 99% level.

The second data set consists of monthly means of basin-averaged ocean bottom pressure using GRACE data, derived from the JPL RL05M mascon time variable gravity field solutions [*Watkins et al.*, 2015]. Comparison with a wide array of BPR measurements demonstrates that this methodology shows significant improvements in the ocean over the regular spherical harmonic GRACE solution, particularly in the tropical and south Atlantic [*Watkins et al.*, 2015]. This is because the constraint system used helps to eliminate correlated errors so that less spatial smoothing is required. Reduced smoothing is especially valuable near to coastlines, an issue of particular importance in a semienclosed basin like the Caribbean Sea. We subtract the global ocean average from the basin average to limit the signal to the dynamical component, as we did in the model analysis (though this makes only a small difference to the results).

The Gaussian-filtered GRACE time series is shown in pink in Figure 3a. It explains 37% of the variance in the altimetry-predicted pressure and has a correlation of 0.63. The top four lagged correlations are at lags of −111, −54, 1, and 59 days, with the expected signs and with the largest correlation (0.63) at 1 day lag. All 132 other lagged correlations have magnitudes smaller than 0.46, showing that the correlation is significant at the 99% level at least. The correlation with the BPR time series is similar at 0.64, showing that the prediction is as good a measure of the basin-averaged bottom pressure as at least one of the observations.

The basin-wide bottom pressure mode therefore exists and bears the same relationship to the propagating sea level mode as was found in the models.

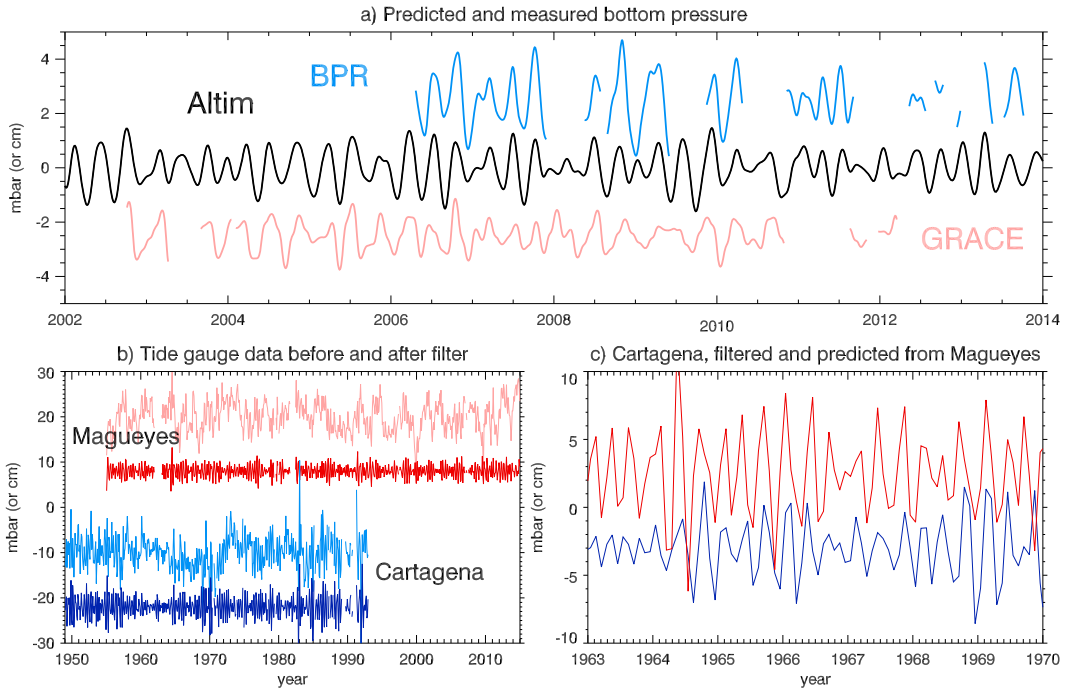

Figure 3. (a) Time series of basin-averaged or point bottom pressure derived from the BPR (blue), predicted based on satellite altimetry (black), and measured by the GRACE satellite (pink). All time series are filtered by taking the difference between a 60 day and a 200 day (twice the width at half maximum) Gaussian smoother, after first removing trend, annual, and semiannual cycles. (b) Time series of bottom pressure at Magueyes (pink) and Cartagena (light blue), with annual, semiannual, and linear trend removed. Red and dark blue are the same after applying a band-pass filter in the 75–175 day period band. (c) Blow up of part of the filtered Cartagena record (blue), and the filtered Magueyes record (red) with a lag and amplitude factor derived from Figure 2 applied to the latter to match it with the Cartagena record.

In contrast to the sea level signal, which tends to have an amplitude which decays toward the coast, the bottom pressure signal in Figure 2d retains much of its amplitude over islands north of the Venezuela basin and reaches some of its largest amplitudes along the coasts of South and Central America. This suggests that in contrast to most mesoscale variability [see *Hughes and Williams*, 2010], the influence of the Caribbean Current instability should be visible in tide gauge records at the coast, where inverse barometer-corrected sea level and bottom pressure are the same thing. Of the many tide gauge records around the Caribbean Sea, two are both long and at relevant locations: Cartagena in Colombia, and Magueyes in Puerto Rico. These have been obtained from the Permanent Service for Mean Sea Level [*Holgate et al.*, 2013], and an inverse barometer correction applied based on the 6-hourly surface atmospheric pressure fields from the National Centers for Environmental Prediction/National Center for Atmospheric Research reanalyses [*Kalnay et al.*, 1996]. The resulting monthly mean time series are shown in Figure 3b after removal of annual and semiannual cycles, and linearly detrending, together with the band-pass filtered versions, using Fourier filtering in this case.

Unfortunately, Cartagena does not overlap in time with the altimetry, but it shows a large variability in the 75–175 day band as predicted by the model data. The spectrum (Figure 1c) shows a sharp peak centered at a 120 day period, with the band-passed time series accounting for 45% of the variance in the 44 year time series (after first removing annual, semiannual, and a linear trend).

The filtered variability at Magueyes is smaller and accounts for only 23% of the nonseasonal, nonsecular variance, but this is also consistent with the model prediction, and the 120 day mode is again clear in the spectrum (Figure 1c). Lagged correlation with altimetry gives strongest correlations of 0.45 at zero lag and −0.48 for a signal arriving in altimetry 56 days before the tide gauge (all 247 peaks in the absolute lagged correlation for altimetry lagging the tide gauge are smaller than 0.36). These lags agree well with Figure 2f, which gives a 3° (1 day) lag at Magueyes. Lagged correlation of filtered Cartagena and Magueyes time series gives a best correlation of 0.36 at a lag corresponding to signals arriving at Cartagena 40 days before Magueyes, which compares well with the lag of 142° (47 days) from Figure 2f. If we use the phase and amplitude factors from Figure 2 to predict Cartagena sea level from Magueyes by applying a lag and gain to the tide gauge data,

we obtain the red curve in Figure 3c (shown for a stretch of the data with no gaps in either tide gauge). Agreement is reasonable, despite the fact that this procedure effectively assumes that the basin mode is the only signal in this frequency band found at either tide gauge, and therefore amplifies errors due to any other variability at Magueyes.

4. Interpretation and Conclusions

The Caribbean Current carries about 20 Sv to the west through the Caribbean Sea and is baroclinically unstable [*Andrade and Barton*, 2000; *Jouanno et al.*, 2008, 2009; *Johns et al.*, 2002]. Satellite altimetry [*Andrade and Barton*, 2000] shows that eddies form in the eastern basin, and travel west before breaking up at the Central American Rise. Modeling studies [*Jouanno et al.*, 2008, 2009] show that the instability, although slightly influenced by North Brazil Current rings and Rossby waves from the wider Atlantic, is intrinsic to the Caribbean Sea and would occur without these influences. Most of the energy is found between periods of about 40 and 200 days [*Jouanno et al.*, 2008, 2009], but there is significant variability of that sea level spectrum within the sea [*Jouanno et al.*, 2008; *Hughes and Williams*, 2010]. The westward propagation speed of a variety of different features is given as 20–30 cm s^{-1} [*Andrade and Barton*, 2000], 15 cm s^{-1} [*Murphy et al.*, 1999] or (in a model) 7–10 cm s^{-1} [*Jouanno et al.*, 2009]. Baroclinic instability therefore generates a broad spectrum of mesoscale variability within the basin, but a particular part of this variability interacts with the basin boundary to produce a sharply peaked spectrum of bottom pressure variability.

The sharp peak is suggestive of a resonant basin mode. As shown by *LaCasce* [2000] and *Cessi and Primeau* [2001], the presence of dissipation has the effect of emphasizing particular modes in which rapidly propagating boundary waves and associated boundary currents play an important role. *LaCasce* [2000], in particular, shows in a one-dimensional case that the resonant modes are simply those for which there are an integer number of wavelengths of the free, long baroclinic Rossby wave across the basin, and the two-dimensional case is very similar for the gravest mode in the meridional direction. That looks very like the case we see here.

Although the basin mode theory assumes quasi-geostrophic dynamics and a vertical sidewall, the same exchange between slow baroclinic Rossby waves and a rapid adjustment along topography has also been shown to occur with finite topography in the planetary geostrophic case [*Marshall*, 2011]. The dynamics are subtle and are explained in more detail in the supporting information, but when applied to our case they mean that a Rossby wave would be absorbed at the western boundary and regenerated at the east, accompanied by the generation of an oscillating boundary current around the basin. This pattern is consistent with what we see in bottom pressure along the southern coast and appears also to generate a secondary Rossby wave as the coast turns to the north along the coast of Colombia (around Cartagena in Figure 1a). In reality, the waves responsible for the boundary adjustment travel at finite speed. The first baroclinic Kelvin wave speed in this basin is 2.2–2.4 m s^{-1} [*Chelton et al.*, 1998], which would imply a lag between east and west of about 10 days or 30° in phase. As we found above, the Rossby wave dispersion relation using the observed wavelength leads to a predicted period close to the observed 120 days. Together with the almost two wavelengths across the basin, this confirms that the mode meets the criteria for a resonant basin mode as described by *LaCasce* [2000]. See the supporting information for further discussion.

Our interpretation is thus that our mode is a resonant basin mode which is excited by baroclinic instability within the Caribbean Sea. This explains why the sea level amplitude of the mode grows toward the west, why the encounter with the Central America Rise produces a rapid response along the South American coast, and why an almost integer number of wavelengths fits across the basin (it may be the basin geometry, or the natural wavelength of the instability process which selects two wavelengths rather than one). As the associated boundary wave interacts with the various gaps in the boundary, it will inevitably cause flows in and out of the basin. As we calculated above, the net inflow and outflow required to explain the basin-averaged pressure signal is only a tiny fraction of the observed changes in flows through individual straits, so we interpret the bottom pressure signal as a side effect of this mode operating in a basin which can exchange mass with the wider ocean.

This is exactly analogous to the operation of a whistle or similar musical instrument. As described by *Jeans* [1937], an organ pipe represents a coupled system in which the instability of a jet of air on encountering an obstacle generates eddies, and those eddies interact with the natural acoustic modes of the organ pipe (in fact *LaCasce* [2000] describes the Rossby basin modes as "like acoustic waves in a clarinet") to excite a resonance in the organ pipe. That resonance results in an audible sound only because the system is open,

allowing mass exchange with the surroundings to radiate a sound wave. In this case, we can "hear" the mode in the oscillations of the Earth's gravity field at a period of 120 days (which corresponds to a note of A♭, many octaves below the audible range).

Acknowledgments
We thank the Permanent Service for Mean Sea Level for providing quality-controlled tide gauge and bottom pressure data, which can be found at http://www.psmsl.org/, and AVISO for provision of the ocean dynamic topography product at http://www.aviso.altimetry.fr/. The ECCO ocean state estimates were provided by the ECCO Consortium for Estimating the Circulation and Climate of the Ocean funded by the National Oceanographic Partnership Program (NOPP). NCEP Reanalysis data were provided by the NOAA/OAR/ESRL PSD, Boulder, Colorado, USA, from http://www.esrl.noaa.gov/psd/. The JPL GRACE Mascon data can be downloaded from http://grace.jpl.nasa.gov. Any other data used in this paper will be supplied by C.W.H. on request by e-mail. This work has been supported by NERC through the National Oceanography Centre, as well as through grant NE/I023384/1. The OCCAM and NEMO models were run and provided by the NOC Southampton modeling group. We thank them and particularly Andrew Coward and Beverly de Cuevas for their help with these data sets.

References

Andrade, C. A., and E. D. Barton (2000), Eddy development and motion in the Caribbean Sea, *J. Geophys. Res.*, *105*, 26,191–26,201, doi:10.1029/2000JC000300.

Blaker, A. T., J. J.-M. Hirschi, G. McCarthy, B. Sinha, S. Taws, R. Marsh, A. Coward, and B. de Cuevas (2014), Historical analogues of the recent extreme minima observed in the Atlantic meridional overturning circulation at 26°N, *Clim. Dyn.*, *44*, 457–473, doi:10.1007/s00382-014-2274-6.

Cessi, P., and F. Primeau (2001), Dissipative selection of low-frequency modes in a reduced-gravity basin, *J. Phys. Oceanogr.*, *31*, 127–137, doi:10.1175/1520-0485(2001)031<0127:DSOLFM>2.0.CO;2.

Chelton, D. B., R. A. deSzoeke, and M. G. Schlax (1998), Geographical variability of the first baroclinic Rossby radius of deformation, *J. Phys. Oceanogr.*, *28*, 433–460, doi:10.1175/1520-0485(1998)028<0433:GVOTFB>2.0.CO;2.

Fukumori, I., O. Wang, W. Llovel, I. Fenty, and G. Forget (2015), A near-uniform fluctuation of ocean bottom pressure and sea level across the deep ocean basins of the Arctic Ocean and the Nordic Seas, *Prog. Oceanogr.*, *134*, 152–172, doi:10.1016/j.pocean.2015.01.013.

Gonzalez, F., E. Bernard, C. Meinig, M. Eble, H. Mofjeld, and S. Stalin (2005), The NTHMP tsunameter network, *Nat. Hazards*, *35*(1), 25–39, doi:10.1007/s11069-004-2402-4.

Holgate, S. J., A. Matthews, P. L. Woodworth, L. J. Rickards, M. E. Tamisiea, E. Bradshaw, P. R. Foden, K. M. Gordon, S. Jevrejeva, and J. Pugh (2013), New data systems and products at the permanent service for mean sea level, *J. Coastal Res.*, *29*, 493–504, doi:10.2112/JCOASTRES-D-12-00175.1.

Hughes, C. W., and V. N. Stepanov (2004), Ocean dynamics associated with rapid J_2 fluctuations: Importance of circumpolar modes and identification of a coherent Arctic mode, *J. Geophys. Res.*, *109*, C06002, doi:10.1029/2003JC002176.

Hughes, C. W., and S. D. P. Williams (2010), The color of sea level: Importance of spatial variations in spectral shape for assessing the significance of trends, *J. Geophys. Res.*, *115*, C10048, doi:10.1029/2010JC006102.

Jeans, J. (1937), *Science and Music*, Cambridge Univ. Press, New York.

Johns, W. E., T. L. Townsend, D. M. Fratantoni, and W. D. Wilson (2002), On the Atlantic inflow to the Caribbean Sea, *Deep Sea Res., Part I*, *49*, 211–243, doi:10.1016/S0967-0637(01)00041-3.

Jouanno, J., J. Sheinbaum, B. Barnier, J.-M. Molines, L. Debreu, and F. Lemarié (2008), The mesoscale variability in the Caribbean Sea. Part I: Simulations and characteristics with an embedded model, *Ocean Modell.*, *23*, 82–101.

Jouanno, J., J. Sheinbaum, B. Barnier, and J.-M. Molines (2009), The mesoscale variability in the Caribbean Sea. Part II: Energy sources, *Ocean Modell.*, *26*, 226–239.

IHO, IOC and BODC (2003), *Centenary Edition of the GEBCO Digital Atlas*, Published on CD-ROM on behalf of the Intergovernmental Oceanographic Commission and the International Hydrographic Organization as part of the General Bathymetric Chart of the Oceans, British Oceanographic Data Centre, Liverpool, U. K.

Kalnay, E., et al. (1996), The NCEP/NCAR 40-year reanalysis project, *Bull. Am. Meteorol. Soc.*, *77*, 437–471.

LaCasce, J. H. (2000), Baroclinic Rossby waves in a square basin, *J. Phys. Oceanogr.*, *30*, 2161–78, doi:10.1175/1520-0485(2000)030<3161:BRWIAS>2.0.CO;2.

Marsh, R., B. A. de Cuevas, A. C. Coward, J. Jacquin, J. J. M. Hirschi, Y. Aksenov, A. J. G. Nurser, and S. A. Josey (2009), Recent changes in the North Atlantic circulation simulated with eddy-permitting and eddy-resolving ocean models, *Ocean Modell.*, *28*(4), 226–239, doi:10.1016/j.ocemod.2009.02.007.

Marshall, D. P. (2011), Rossby wormholes, *J. Mar. Res.*, *69*, 309–330, doi:10.1357/002224011798765213.

Menemenlis, D., I. Fukumori, and T. Lee (2005a), Using Green's functions to calibrate an ocean general circulation model, *Mon. Weather Rev.*, *133*(5), 1224–1240, doi:10.1175/MWR2912.1.

Menemenlis, D., et al. (2005b), NASA supercomputer improves prospects for ocean climate research, *Eos Trans. AGU*, *86*, 89–96.

Murphy, S. J., H. E. Hurlburt, and J. J. O'Brien (1999), The connectivity of eddy variability in the Caribbean Sea, the Gulf of Mexico and the Atlantic Ocean, *J. Geophys. Res.*, *104*, 1431–1452, doi:10.1029/1998JC900010.

Peralta-Ferriz, C., J. H. Morison, J. M. Wallace, and J. L. Zhang (2011), A basin-coherent mode of sub-monthly variability in Arctic Ocean bottom pressure, *Geophys. Res. Lett.*, *38*, L14606, doi:10.1029/2011GL048142.

Volkov, D. L., and F. W. Landerer (2013), Nonseasonal fluctuations of the Arctic Ocean mass observed by the GRACE satellites, *J. Geophys. Res. Oceans*, *118*, 6451–6460, doi:10.1002/2013JC009341.

Watkins, M. M., D. N. Wiese, D.-N. Yuan, C. Boening, and F. W. Landerer (2015), Improved methods for observing Earth's time variable mass distribution with GRACE using spherical cap mascons, *J. Geophys. Res. Solid Earth*, *120*, 2648–2671, doi:10.1002/2014JB011547.

Williams, J., C. W. Hughes, M. E. Tamisiea, and S. D. P. Williams (2014), Weighing the ocean with bottom-pressure sensors: Robustness of the ocean mass annual cycle estimate, *Ocean Sci.*, *10*, 701–718, doi:10.5194/os-10-701-2014.